

Model Predictive Control based AGC for Multi-Terminal DC grids

Paul Mc Namara, *Member, IEEE*, Álvaro Ortega, *Student Member, IEEE*, Federico Milano, *Senior Member, IEEE*
 Electricity Research Centre, Engineering and Materials Science Centre, University College Dublin, Belfield, Dublin.
 Email: paul.mcnamara@ucd.ie, alvaro.ortega-manjavacas@ucdconnect.ie, federico.milano@ucd.ie

Abstract—With increasing DC grid connections between non-synchronous AC systems it is desirable that DC connections would take a role in frequency regulation for connected AC grids. A number of primary and secondary P and PI based controllers have been designed previously for this purpose. Here Model Predictive Control is proposed for including DC power controllers in the provision of Automatic Generation Control.

I. INTRODUCTION

In recent years interest in High Voltage DC (HVDC) grids has steadily increased as the need to transport large volumes of renewable energy over large distances in electrical grids worldwide continues to grow. In Europe, for example, a large interconnected grid or “Supergrid” is planned such that electrical energy can be moved across the continent [1]. The rationale involved is that by interconnecting renewable energy sources over large areas it allows the aggregation of the stochastic renewable energy supply, thus ensuring greater reliability of the renewable supply across electrical grids.

Multi-terminal HVDC (MTDC) grids, are HVDC grids in which multiple HVDC lines can enter an individual DC voltage node. For the construction of MTDC grids Voltage Source Converter (VSC) technology allows bidirectional power flows on lines (unlike Line Commutated Converter technology), and thus VSC-based MTDC grids allow a great degree of flexibility in terms of how power can be transferred using a DC grid. This flexibility, combined with a VSC’s ability to independently control real and reactive power, is what promises to make VSC-HVDC the backbone of future DC power transmission systems [2].

As DC interconnection in an AC system increases, there is a consequent decrease in the AC system inertia. This means have been sought so as allow DC connections to react to frequency deviations in a similar manner to AC systems [2]. Additionally, by allowing DC connections to respond to frequency events, AC areas connected by DC links can collectively respond to frequency events in individual areas, and as a result can make more efficient use of reserves [3]. Thus a range of primary and secondary frequency control algorithms have been proposed to allow VSCs to contribute to frequency regulation in AC systems [2], [4]–[7].

Typically, these controllers have been based on decentralised PI approaches. Model Predictive Control (MPC) is a multi-input multi-output, optimisation-based control technique, and is capable of explicitly considering system constraints. MPC

has been shown to provide several advantages in terms of performance over PI controllers in systems with high penetrations of renewable sources [8], and has previously considered point-to-point DC links for use in Automatic Generation Control (AGC), on a simulated model of the European grid [9].

Centralised MPC, decentralised communication-free MPC, and distributed MPC approaches have been proposed for AGC in MTDC systems in [10], [11]. The approaches in [10], [11] are based on the direct manipulation of the DC voltages using MPC, at a secondary control level, in order to manipulate the powers transferred between areas. Typically, however, VSCs receive a DC power setpoint message from TSOs in order to manipulate the DC power, and this setpoint is sent to other lower level controllers to control the DC voltages.

Thus, in this paper, MPC is used to control the power setpoint in a number of VSCs’ primary frequency controller in order to coordinate power transfers over an MTDC grid to aid AGC in AC areas connected to the DC grid. The paper is constructed as follows: the modelling of the DC system and VSCs are given in Section II. The application of MPC to coordinate AGC in AC areas connected to the MTDC grid is described in Section III. Simulations and results are given in Section IV-B. Finally, the conclusions are given in Section V.

II. MODELLING

In this section the modelling and control of the VSCs and the DC network are outlined. These are described in greater detail in [2].

The j^{th} ideal VSC, acting as an interface between an AC grid and the j^{th} MTDC voltage node in a larger DC system, is portrayed in Fig. 1. The following equality applies across the ideal VSC:

$$v_{dcj}i_{dcj} = v_{t,aj}i_{t,aj} + v_{t,bj}i_{t,bj} + v_{t,cj}i_{t,cj} \quad (1)$$

where v_{dcj} and i_{dcj} represent the DC voltage and current entering the j^{th} VSC from the DC grid, respectively, $v_{t,aj}$, $v_{t,bj}$, and $v_{t,cj}$ are the sinusoidally varying a, b, and c phase voltages produced on the AC side of the VSC, respectively, and $i_{t,aj}$, $i_{t,bj}$, and $i_{t,cj}$ are the sinusoidally varying a, b, and c phase currents produced on the AC side of the VSC, respectively.

The power balance between the DC and AC sides of the converter is given by:

$$p_{acj} + v_{dcj}i_{dcj} - p_{lossj} - \frac{1}{2}C_{dcj} \frac{d(v_{dcj}^2)}{dt} = 0, \quad (2)$$

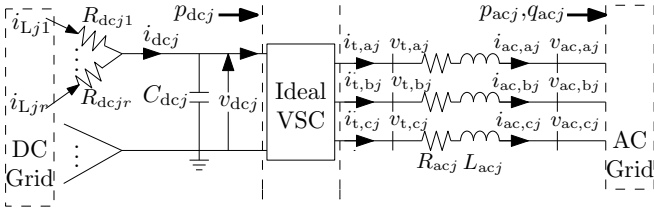


Fig. 1. Block diagram of the j^{th} ideal VSC acting as an interface between an AC grid and MTDC grid voltage node.

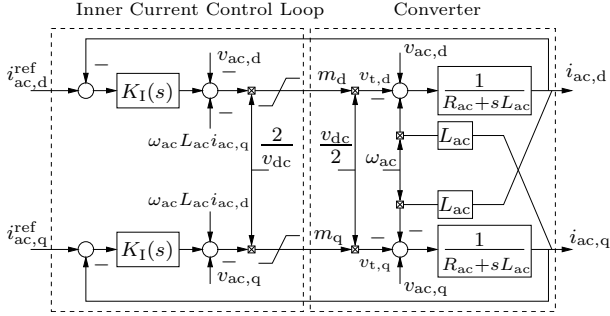


Fig. 2. Block diagram of the VSC inner control loop and converter in dq form.

where $p_{acj} = \frac{1}{2}(v_{ac,dj}i_{ac,dj} + v_{ac,qj}i_{ac,qj})$, $v_{ac,dj}$ and $v_{ac,qj}$ are AC side voltages represented in the dq rotating frame, and $i_{ac,dj}$ and $i_{ac,qj}$ are AC side currents represented in the dq rotating frame; the $\frac{1}{2}C_{dcj}\frac{d(v_{dcj}^2)}{dt}$ term represents energy variations in the DC side capacitor, where C_{dcj} is the capacitance across the j^{th} VSC's DC voltage node, and $p_{loss} = \frac{3}{2}R_{acj}i_{acj}^2$ is the circuit losses of the converter, where R_{acj} represents the ohmic power loss of the inductor, and $i_{acj}^2 = i_{ac,dj}^2 + i_{ac,qj}^2$. Switching losses in the VSC are ignored here.

The DC side dynamics are given as follows:

$$C_{dcj} \frac{d}{dt} v_{dcj} = i_{dcj}, \quad (3)$$

where the DC side current $i_{dcj} = \sum_{h=1}^r i_{Ljh}$; the current travelling on the DC line between DC voltage nodes j and h is given by $i_{Ljh} = \frac{1}{R_{dcjh}}(v_{dch} - v_{dcj})$, and R_{dcjh} is the resistance in the line connecting DC voltage nodes j and h .

Fig. 2 shows the block diagram of both the VSC converter and its inner loop controller [2]. For compactness, j subscripts are dropped in the following description of VSC j 's dynamics, and in Fig. 2. The converter equations are represented in the dq-frame as follows:

$$\begin{aligned} R_{ac}i_{ac,d} + L_{ac} \frac{di_{ac,d}}{dt} &= \omega_{ac}L_{ac}i_{ac,q} + v_{ac,d} - v_{t,d} \\ R_{ac}i_{ac,q} + L_{ac} \frac{di_{ac,q}}{dt} &= -\omega_{ac}L_{ac}i_{ac,d} + v_{ac,q} - v_{t,q} \end{aligned} \quad (4)$$

where L_{ac} represents the inductance of the AC side filter, and $v_{t,d}$ and $v_{t,q}$ are the pre-filtered AC voltages produced by the VSC. Capacitors are typically employed to filter AC output

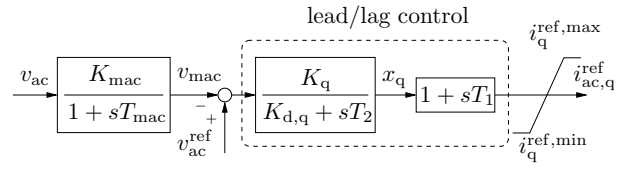


Fig. 3. The outer AC voltage controller.

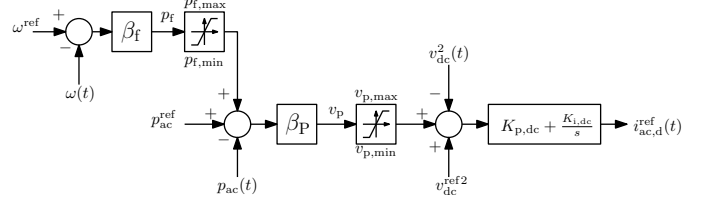


Fig. 4. The primary frequency controller of the VSC HVDC modules.

harmonics. As higher dynamics are not considered in the AC output here, these capacitor dynamics are ignored.

The controller $K_I(s)$ in Fig. 2 is a PI controller with the following transfer function:

$$K_I(s) = \frac{R_{ac} + sL_{ac}}{sT_1} \quad (5)$$

where T_1 is the time constant of the first order response of the closed-loop step response of the current control loops.

The use of a Phase Locked Loop (PLL) enables the representation the VSC dynamics in a synchronous framework and significantly simplifies control design by allowing the independent manipulation of p_{ac} and q_{ac} . As the PLL dynamics occur on significantly faster time scales than those of interest in this paper, they are considered as algebraic, which in turn implies $v_{ac,d} = V_{ac}(t)$ and $v_{ac,q} = 0$, where $V_{ac}(t)$ is the instantaneous peak of the grid (line-to-neutral) voltage. This enables independent control of p_{ac} and q_{ac} in a straightforward manner.

The magnitude of the ac voltage v_{ac} at the point of connection to the grid is regulated, as in Fig. 3, via manipulation of $i_{ac,q}^{\text{ref}}$. In this paper a primary frequency controller is used to allow the VSC respond to variations in its local frequency via manipulation of the power injected by the VSC to the AC grid. This controller, given in Fig. 4, manipulates $i_{ac,d}^{\text{ref}}$ in order to control p_{ac} . The controller can be tuned to trade off the conflicting grid objectives of regulation of the frequency, tracking of the scheduled power transfer from the DC to the AC grid p_{ac}^{ref} , and regulation of the voltage about it's operating point.

In this paper a 6th order Marconato synchronous machine is used to model the synchronous generators [12]. The following simplified frequency model (which is used now simply for illustrative purposes) describes how the frequency is influenced where there are ρ sources of power in the synchronous area:

$$\frac{d}{dt} \omega(t) = \frac{1}{M} \left(\sum_{j=1}^{\rho} p_{inj}(t) - p_L(t) - D(\omega(t) - \omega_{ac}) \right) \quad (6)$$

where M represents the inertia of the generator, $\omega(t)$ is the frequency, $p_{inj}(t)$ is the j^{th} source of power in the synchronous area, $p_L(t)$ represents the current power load in the system at time t , and D is a damping coefficient. This illustrates that the key to accurate frequency control is the coordinated control of the power sources. Through the use of MPC it is possible to use the system model in order to manipulate the power setpoints of both the generators and the VSC HVDC frequency controller in order to provide high performance frequency control.

III. MODEL PREDICTIVE CONTROL FOR AGC IN MTDC NETWORKS

A. Model Predictive Control

Model Predictive Control is an optimisation based control technique that uses state-space based predictions in order to form optimal inputs to a system over a prediction horizon. While inputs are calculated over the full prediction horizon, only the input for the first sample step of the prediction horizon is applied to the system, and this process is repeated every sample step.

A discrete-time, linear, time-invariant state-space model for a system is given by

$$\mathbf{x}(k+1) = \mathbf{A}\mathbf{x}(k) + \mathbf{B}\mathbf{u}(k) \quad (7)$$

$$\mathbf{y}(k) = \mathbf{C}\mathbf{x}(k), \quad (8)$$

where $\mathbf{x}(k)$, $\mathbf{u}(k)$, and $\mathbf{y}(k)$ are the states, inputs, and outputs of the system at sample step k , respectively. Matrices \mathbf{A} , \mathbf{B} , and \mathbf{C} are the relevant state-space matrices. An augmented state-space model allows these equations to be framed in terms of $\Delta\mathbf{u}(k)$ and the augmented state $\boldsymbol{\chi}(k) = [\Delta\mathbf{x}^T(k) \ \mathbf{x}^T(k)]^T$ (for a general variable $b(k)$, $\Delta b(k) = b(k) - b(k-1)$, i.e., the Δ operator denotes the change in a variable between sample steps $k-1$ and k), which ensures integral action in the controller. This is given as follows:

$$\boldsymbol{\chi}(k+1) = \hat{\mathbf{A}}\boldsymbol{\chi}(k) + \hat{\mathbf{B}}\Delta\mathbf{u}(k) \quad (9)$$

$$\mathbf{y}(k+1) = \hat{\mathbf{C}}\boldsymbol{\chi}(k+1), \quad (10)$$

where $\hat{\mathbf{A}}$, $\hat{\mathbf{B}}$, and $\hat{\mathbf{C}}$ are the incremental state-space matrices. The predicted state $\tilde{\mathbf{x}}(k+1)$ and incremental predicted state $\Delta\tilde{\mathbf{x}}(k+1)$ can be found from these equations, where for a general vector \mathbf{p} , its prediction vector is $\tilde{\mathbf{p}}(k) = [\mathbf{p}^T(k) \ \dots \ \mathbf{p}^T(k+H-1)]^T$, where H is called the prediction horizon for the system [13].

MPC problems are constructed to fulfill control objectives for a system based on knowledge of $\mathbf{x}(k)$. A cost function, $J(\boldsymbol{\chi}(k), \Delta\tilde{\mathbf{u}}(k))$ (which will henceforth be denoted by $J(k)$), is designed so as to embody the system's objectives. Typically this cost function is quadratic in $\Delta\tilde{\mathbf{u}}$ and in this paper the cost function takes the following form:

$$\begin{aligned} J(k) &= \tilde{\mathbf{e}}^T(k+1)\mathbf{Q}_e\tilde{\mathbf{e}}(k+1) + \Delta\tilde{\mathbf{u}}^T(k)\mathbf{Q}_u\Delta\tilde{\mathbf{u}}(k) \\ &= \Delta\tilde{\mathbf{u}}^T\mathbf{G}\Delta\tilde{\mathbf{u}} + \Delta\tilde{\mathbf{u}}^T\mathbf{f} + \mu, \end{aligned} \quad (11)$$

where the error vector, $\mathbf{e}(k) = \mathbf{y}(k) - \mathbf{r}(k)$, and $\mathbf{r}(k)$ are the setpoints of subsystem a at sample step k . Following straightforward matrix manipulation it can be shown that $\mathbf{G} = \hat{\mathbf{B}}^T\hat{\mathbf{C}}^T\mathbf{Q}_e\hat{\mathbf{C}}\hat{\mathbf{B}} + \hat{\mathbf{Q}}_u$, where \mathbf{G} is a square symmetric non-singular matrix, $\mathbf{f} = \mathbf{K}_\chi\boldsymbol{\chi}(k) - \mathbf{K}_r\tilde{\mathbf{r}}(k)$, where $\mathbf{K}_\chi = 2\hat{\mathbf{B}}^T\hat{\mathbf{C}}^T\mathbf{Q}_e\hat{\mathbf{C}}\hat{\mathbf{A}}$ and $\mathbf{K}_r = 2\hat{\mathbf{B}}^T\hat{\mathbf{C}}^T\mathbf{Q}_e$ are constant matrices. The constant μ represents terms that do not depend on $\Delta\tilde{\mathbf{u}}(k)$.

The weighting matrices \mathbf{Q}_e , and \mathbf{Q}_u determine the relative importance of minimising errors and the incremental changes in inputs, respectively. For the unconstrained case, an analytical solution for the inputs can then be found by finding the value of $\Delta\tilde{\mathbf{u}}(k)$ that minimises $J(k)$.

The optimal choice of controls $\Delta\tilde{\mathbf{u}}^*(k)$ is obtained when,

$$\frac{\partial}{\partial\Delta\tilde{\mathbf{u}}(k)}J(k) = 2\mathbf{G}\Delta\tilde{\mathbf{u}}(k) + \mathbf{f} = 0, \quad (12)$$

where a superscripted $*$ denotes the optimum value of a variable. This yields the solution,

$$\begin{aligned} \Delta\tilde{\mathbf{u}}^*(k) &= -\frac{1}{2}\mathbf{G}^{-1}\mathbf{f} \\ &= -\frac{1}{2}\mathbf{G}^{-1}(\mathbf{K}_\chi\boldsymbol{\chi}(k) - \mathbf{K}_r\tilde{\mathbf{r}}(k)) \end{aligned} \quad (13)$$

Thus the control law is effectively a fixed gain feedback law and can be computed in a highly efficient fashion. While in this paper the unconstrained case is considered, it is possible to implicitly consider system constraints in the MPC formulation by forming a constrained optimisation problem from (11). The input at the start of the horizon $\mathbf{u}(k)$ is applied to the system and this process is repeated each sample step. Unconstrained MPC in this form is equivalent in performance to a finite horizon Linear Quadratic Regulator.

B. Using MPC for AGC

In order to use MPC for AGC in MTDC systems the following steps are carried out:

- A continuous-time state-space model is derived for the system by linearising the system about its nominal operating point, as derived from the load flow for the system. This is given by:

$$\frac{d}{dt}\mathbf{x}(t) = \mathbf{A}\mathbf{x}(t) + \mathbf{B}\mathbf{u}(t) \quad (14)$$

$$\mathbf{y}(k) = \mathbf{C}\mathbf{x}(k), \quad (15)$$

In this case $\mathbf{x}(t)$ are continuous states that are either measured or estimated. The inputs $\mathbf{u} = [p_{m,mpc1}^{\text{ref}}, \dots, p_{m,mpcn_g}^{\text{ref}}, p_{ac,mpc1}^{\text{ref}}, \dots, p_{ac,mpcn_{vsc}}^{\text{ref}}]$, where $p_{m,mpcj}^{\text{ref}}$ is the j^{th} generator setpoint controlled by MPC, where there are n_g generator setpoints controlled by MPC, and $p_{ac,mpcj}^{\text{ref}}$ is the j^{th} VSC scheduled power setpoint that is controlled by MPC, where there are n_{vsc} VSC scheduled power setpoint controlled by MPC. The outputs $\mathbf{y}(t) = [\omega_{mpc1}, \dots, \omega_{mpcn_g}]$, where ω_{mpcj} is the frequency of the j^{th} generator controlled by MPC, where there are n_g generators controlled by MPC.

- The continuous-time state-space (14) is discretised using a Zero Order Hold discretisation in order to give the discrete-time state-space model (14).
- Then MPC can be used to calculate $u(k)$ at each sample step.

IV. SIMULATION AND RESULTS

In order to illustrate the application of MPC for AGC in MTDC connected AC grids a simulation was constructed. The simulation setup and results are described in this section.

A. Simulation setup

The testbed is taken from [2] and involves 3 asynchronous AC areas connected an MTDC grid, as in Fig. 5. The simulation was built using the Dome software package [14]. The base power is given by $S_{\text{base}}=100$ MW, base voltage $V_{\text{base}} = 470$ kV, and base frequency $\omega_{\text{ac}} = 50$ Hz. After load flow the initial generator values are given by: $P_{m1}^0 = 7.02$ pu, $P_{m2}^0 = 7.01$ pu, $P_{m3}^0 = 9.98$ pu, $P_{m4}^0 = 7.02$ pu, $P_{m5}^0 = 9.07$ pu, and $P_{m6}^0 = 2.96$ pu, where P_{mj} is the initial power output in pu of generator j , and p^0 denotes the initial value of a variable p ; initial DC voltages were given by $v_{\text{dc}1}^0 = 1$ pu, $v_{\text{dc}2}^0 = 0.998$ pu, $v_{\text{dc}3}^0 = 0.9986$ pu, and $v_{\text{dc}4}^0 = 1.0014$. For generators 1 and 2, $M = 13$ s, and for generators 3 to 6, $M = 12.35$ s. On the DC lines $R_{\text{dc}ij} = 1.5 \Omega$, and $C_{\text{dc}j} = 0.4$ mF for all feasible i and j . There are 3 loads in Area 1 on buses 7, 8, and 9 as shown in Fig.

For the primary frequency control of the VSC controllers $\beta_{f1} = \beta_{f4} = 1$, with $\beta_{P1} = \beta_{P4} = 0.1$, while $\beta_{f2} = \beta_{f3} = 5$, with $\beta_{P2} = \beta_{P3} = 0.5$, and $K_{p,\text{dc}j} = K_{i,\text{dc}j} = 1$, for $j = 1, \dots, 4$. Thus greater emphasis is placed on frequency control in VSCs 2 and 3 connected to the main AC grid, and the VSCs connected to the the smaller grids, 1 and 4, concentrate on regulating the DC voltage to near it's nominal value. The droop controllers in all generators are given a gain of $K_d = 0.05$.

The MPC controllers are used to control the power setpoints in all 4 VSCs and for generators 1-4. Generators 5 and 6 use regular PI controllers to regulate their generators with an integral gain of 20. A sample time of $T_s = 0.2$ s was used for the MPC controller with $H = 50$. The weighting matrices are given by $Q_e = \text{diag}(2, \dots, 2)$ and $Q_u = \text{diag}(0.01, \dots, 0.01)$. 5.

B. Results

Two simulations were conducted for comparison purposes. An MPC simulation was conducted using the MPC parameters as described in the previous subsection. Another simulation was conducted using one PI controller, with a gain of 20, per AC area for the implementation of AGC. The local Center of Inertia (COI) measurement was used as the input to the PI. The simulation scenario that was conducted involved the disconnection of the load on bus 8.

The frequency responses for the COI of AC area 1 under both MPC and PI control are given in Fig. 6. It can be seen that the MPC reduces the size of the initial deviation of the frequency in comparison to the PI. It can be seen that there is

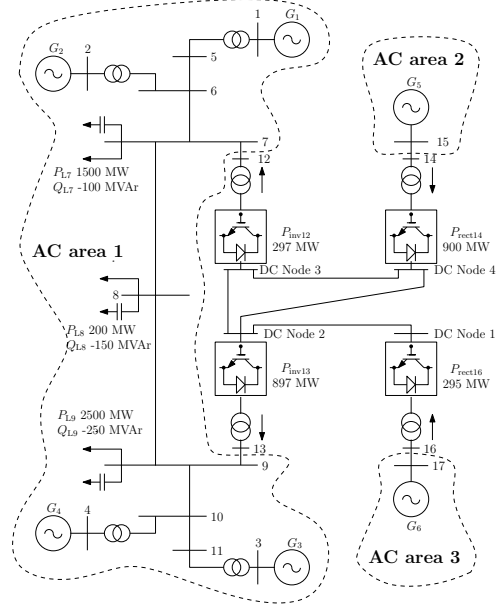


Fig. 5. Testbed with 3 asynchronous areas separated by a DC grid [2].

an increase in frequency in AC areas 2 and 3 after load 8 is disconnected as power is transferred from AC area 1 to areas 2 and 3. For clarity the responses in AC areas 2 and 3 for the PI response are omitted as these are quite similar to those given under MPC.

It can be seen in Fig. 7 that the trade off for the improvement in frequency response is a larger deviation of the DC voltage from it's nominal value. It is necessary that at the tuning phase, the trade off between the frequency response and the voltage deviation is carefully considered as it is necessary for the DC voltage to stay close to it's original value for proper operation of the DC grid [2].

The deviation of the DC powers injected into the AC grid from their nominal values can be seen in Fig. 8. As would be expected in this case, it can be seen that VSCs 2 and 3 choose to inject more power into the DC grid after the load loss, in order to reduce the amount of AC power in AC area 1, and then VSCs 1 and 4 absorb this extra power. This response is reflected in Fig. 9, where it can be seen that $p_{\text{dc}2}^{\text{ref}}$ and $p_{\text{dc}3}^{\text{ref}}$ are lowered in order to reduce the power AC Area 1 receives from the DC grid.

Thus, from these results it can be seen how MPC is capable of coordinating the input responses on the DC and AC grid in order to improve the frequency response in the AC system in comparison to a PI-based approach.

V. CONCLUSIONS

In this paper MPC has been proposed for performing AGC in AC grids that are connected to MTDC grids. The results show that an improvement in the dynamic frequency response is achieved through the use of MPC versus a PI controller. Future work will consider communication delays, and the application of MPC in a stochastic framework, such that

renewables such as wind and solar can be explicitly considered in the control formulation.

ACKNOWLEDGMENT

Paul Mc Namara and Federico Milano are funded under the Programme for Research in Third Level Institutions and co-funded under the European Regional Development Fund (ERDF). F. Milano is also supported by the EC Marie Skodowska-Curie Career Integration Grant No. PCIG14-GA-2013-630811. 200.0. Álvaro Ortega is funded by the Science Foundation Ireland under Grant No. SFI/09/SRC/E1780. The opinions, findings and conclusions or recommendations expressed in this material are those of the authors and do not necessarily reflect the views of the Science Foundation Ireland.

REFERENCES

- [1] T. Houghton, K. Bell, and M. Doquet, "The economic case for developing HVDC-based networks to maximise renewable energy utilisation across Europe: an advanced stochastic approach to determining the costs and benefits," *CIGRE*, 2012.
- [2] N. Chaudhuri, B. Chaudhuri, R. Majumder, and A. Yazdani, *Multi-terminal Direct-current Grids: modeling, analysis, and control*. John Wiley & Sons, 2014.
- [3] J. Dai, "Frequency control coordination among non-synchronous AC areas connected by a multi-terminal HVDC grid," Ph.D. dissertation, Supélec, France, 2011.
- [4] J. Dai, Y. Phulpin, A. Sarlette, and D. Ernst, "Coordinated primary frequency control among non-synchronous systems connected by a multi-terminal high-voltage direct current grid," *IET Generation, Transmission, Distribution*, vol. 6, no. 2, pp. 99–108, 2012.
- [5] M. Andreasson, R. Wiget, D. Dimarogonas, and K. A. G. Johansson, "Distributed primary frequency control through multi-terminal HVDC transmission systems," *arXiv preprint arXiv:1409.8013*, 2014.
- [6] M. Andreasson, R. Wiget, D. Dimarogonas, K. Johansson, and G. Andersson, "Distributed secondary frequency control through multi-terminal HVDC transmission systems," in *Proceedings of the IEEE Conference on Decision and Control*, Osaka, Japan, 2015.
- [7] A. Egea-Alvarez, J. Beerten, D. Van Hertem, and O. Gomis-Bellmunt, "Primary and secondary power control of multiterminal HVDC grids," in *Proceedings of the 10th IET International Conference on AC and DC Power Transmission*, Dec 2012, pp. 1–6.
- [8] A. Ersdal, L. Imsland, and K. Uhlen, "Model Predictive Load-Frequency Control," *accepted for publication in IEEE Transactions on Power Systems*, 2015.
- [9] A. Fuchs, M. Imhof, T. Demiray, and M. Morari, "Stabilization of large power systems using VSC–HVDC and Model Predictive Control," *IEEE Transactions on Power Delivery*, vol. 29, no. 1, pp. 480–488, 2014.
- [10] P. Mc Namara, R. Meere, T. O'Donnell, and S. McLoone, "Control strategies for Automatic Generation Control over multi-terminal HVDC grids," *submitted to the International Journal of Electrical Power and Energy Systems*, preprint available at: <http://ercdocuments.ucd.ie/dms/public/MTDCLFCMPCELS.pdf>, 2015.
- [11] P. Mc Namara, R. R. Negenborn, B. de Schutter, G. Lightbody, and S. McLoone, "Distributed MPC for frequency regulation in multi-terminal HVDC grids," *Control Engineering Practice*, vol. accepted for publication, 2015.
- [12] F. Milano, *Power system modelling and scripting*. Springer Science & Business Media, 2010.
- [13] J. Maciejowski, *Predictive Control with Constraints*. Harlow, England: Prentice Hall, 2002.
- [14] F. Milano, "A python-based software tool for power system analysis," in *IEEE Power and Energy Society General Meeting (PES)*, 2013, pp. 1–5.

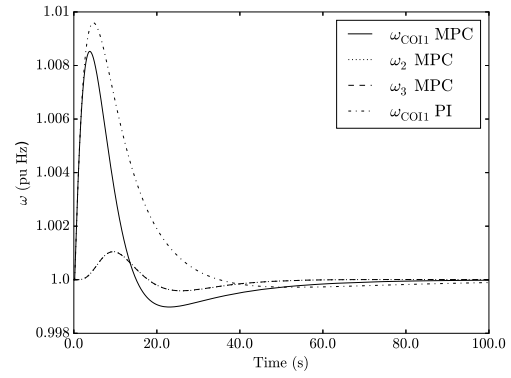


Fig. 6. Frequencies for each generator after the load disturbance.

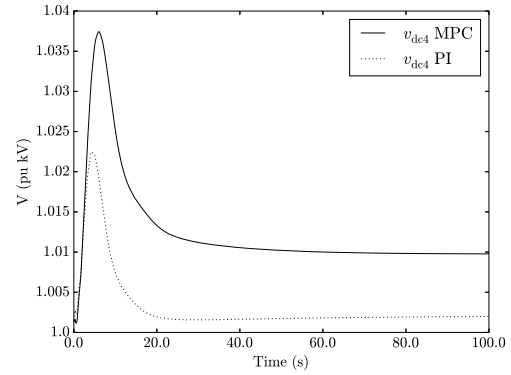


Fig. 7. DC voltage at each DC node after power load disturbance.

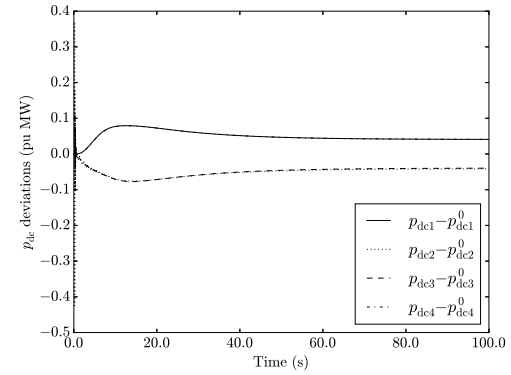


Fig. 8. Deviations of the powers injected into the DC grid at each VSC about their nominal starting positions.

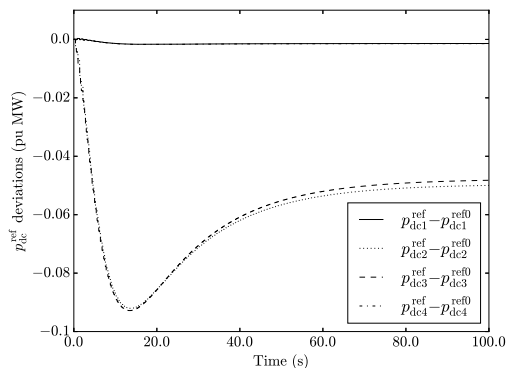


Fig. 9. Deviation of the power setpoints sent to each VSC about their nominal starting positions.